Applied Thermal Engineering 215 (2022) 119000

Contents lists available at ScienceDirect

Applied Thermal Engineering

journal homepage: www.elsevier.com/locate/apthermeng

Research Paper

Theoretical evaluation of adsorption desalination performance of metal-organic frameworks under varying scenarios

Yichen Wang [a,b], Xiaoxiao Xia [a], Dongchen Shen [a], Zhengkai Tu [a], Xiaobing Luo [a,b], Song Li [a,b,*]

[a] Department of New Energy Science and Engineering, School of Energy and Power Engineering, Huazhong University of Science and Technology, Wuhan 430074, China
[b] China-EU Institute for Clean and Renewable Energy, Huazhong University of Science and Technology, Wuhan 430074, China

ARTICLE INFO

Keywords:
Adsorption characteristics
Adsorption isotherms
Water production
Performance ratio

ABSTRACT

Adsorption desalination systems (ADs) driven by low-grade energy are regarded as sustainable alternatives to address water shortages due to their low energy consumption. Adsorbents is the key materials for the performance of ADs. In this work, a numerical study was performed to assess the water production performance of ADs based on metal–organic frameworks (MOFs) and other adsorbents under different working conditions. It is found that the trends in specific daily water production (SDWP) and performance ratio (PR) with hot and chilled water temperature are closely correlated with the adsorption characteristics, i.e., water uptake and the shape of adsorption isotherms. Moreover, considering both SDWP and PR, MOFs outperform other adsorbents owing to their high water transfer amount per cycle under various conditions. Among 12 adsorbents, DUT-67, Al-fumarate and MIL-100(Fe) are the top performers at chilled water temperature of 10 °C, 20 °C and 30 °C respectively with average SDWP (PR) of 3.31 m^3/ton/day (0.33), 8.05 m^3/ton/day (0.56) and 13.46 m^3/ton/day (0.71), increased by 43.8% (32.0%), 65.3% (40%), and 102.7% (44%) compared to traditional silica gel. This work provides helpful insights into the correlation between desalination performance and water adsorption characteristics of adsorbents under varying working conditions, which favors choosing and designing of potential adsorbents for ADs.

1. Introduction

Global population growth and the expansion of agricultural and industrial activities have accelerated the depletion of water resources. It was estimated that global water demand would increase by 3–4% annually [1], and two billion people will suffer from drinking water shortages by 2025 [2]. The freshwater available for human accounts for only 2.5% of the total water on earth, while 97.5% as saline water [3]. Three commercial desalination technologies, including multi-stage flash evaporation (MSF), multi-effect distillation (MED) and reverse osmosis (RO), account for 90% of the total installed capacity [4]. Nevertheless, these energy-intensive desalination technologies increase carbon footprint due to the enormous consumption of fossil fuels [3]. Besides, the inherent fouling and corrosion problems of MSF and MED impose additional requirements on equipment materials, while the RO membrane clogging issue reduces the device's lifetime [1,5]. Recently, the sustainable adsorption desalination system (ADs) that is expected to address the above problems has attracted growing research interests.

In an AD system, the distilled water is yielded by the amalgamation of "adsorption-driven evaporation" and "desorption-driven condensation" processes. Most adsorbents can be regenerated by low-temperature heat sources, hence ADs are driven by low-grade thermal energy (60–90 °C [6]) such as industrial waste heat or renewable energy that favors the remarkable reduction in carbon footprint [7]. In particular, ADs can produce both cooling power and high-quality water (Total Dissolved Solids < 10 ppm [8,9]) simultaneously. In addition, the low evaporation temperature is favorable for the reduced fouling and corrosion in the evaporator compared to MED [8]. Thus, competitive advantages of ADs are highlighted, namely, (a) powered by low-grade thermal energy, (b) co-generation of desalinated water and cooling, and (c) reduced fouling and corrosion. However, the water production performance of ADs is still unsatisfactory currently, restricting their wide applications. In order to improve the specific daily water

Abbreviations: ADs, Adsorption Desalination system; SDWP, Specific Daily Water Production, m^3/(ton·day); LDF, Linear Driving Force; LMTD, Log Mean Temperature Difference; MOFs, Metal-Organic Frameworks; MED, Multi-Effect Distillation; MSF, Multi-Stage Flash evaporation; RO, Reverse Osmosis; PR, Performance Ratio; DVS, Dynamic Vapor Sorption.

* Corresponding author.
E-mail address: songli@hust.edu.cn (S. Li).

https://doi.org/10.1016/j.applthermaleng.2022.119000
Received 15 March 2022; Received in revised form 7 June 2022; Accepted 8 July 2022
Available online 12 July 2022

Nomenclature

c_p	Specific heat capacity, J/(kg·K)
D_s	Surface diffusion coefficient, m^2/s
D_{so}	Pre-exponential constant, m^2/s
E_a	Activation energy, J/mol
F	Fractional uptake
F_o	Geometric parameter
h	Enthalpy, J/kg
h_{fg}	Water latent heat, J/kg
k_0	LDF model empirical constant, 1/s
M	Mass, kg
m	Mass flow rate, kg/s
P	Pressure, Pa
P_s	Saturated pressure, Pa
Q_{st}	Isosteric heat of adsorption, J/kg
R	Ideal gas constant, J/(mol·K)
R_p	Radius of the particle, m
T	Temperature, K
t_{cycle}	Cycle time, s
U	Overall heat transfer coefficient, $W/(m^2·K)$
W(0)	Initial water uptake, kg/kg
W(∞)	Equilibrium water uptake, kg/kg
W(t)	Transient water uptake, kg/kg
ΔW(t)	Water transfer amount, kg/kg

Subscripts

ad	Adsorbent
ads	Adsorption
b	Brine
cond	Condenser
chilled	Chilled water
cooling	Cooling water
d	Desalinated water
des	Desorption
evap	Evaporator
s	Seawater
hx	Heat exchanger
hot	Hot water
v	Vapor
w	Water

Symbols

i	Adsorption or desorption process
j	Cooling or hot water
φ	Operation status controller
τ	Number of cycles per day

production (SDWP) and performance ratio (PR), many efforts have been devoted to the following three aspects: (1) advanced system configuration, (2) optimum operating strategy and (3) more superior adsorbents. In terms of advanced system configuration, the ADs with different number of adsorption beds, stages, evaporators/condensers as well as cycles with heat or mass recovery have been studied. For example, the enhanced performance by applying mass recovery between beds in the ADs has been demonstrated experimentally and numerically compared to the conventional configuration without mass recovery [10]. Thu et al. [11] experimentally compared the water production performance of the ADs in two-bed and four-bed operation modes under different hot water temperatures. The results showed that the SDWP of four-bed operation mode is significantly higher than that of two-bed operation mode at high hot water temperature. Further,they proposed an advanced ADs with internal heat recovery between evaporator and condenser using an encapsulated evaporator-condenser unit [12] by numerical study. It was found that the evaporation pressure was raised due to the direct heat recovery from the condenser, resulting in the water production rates improved by three folds of the conventional configuration. In terms of optimum operating strategy, numerous studies have reported that operating conditions such as cycle time, hot water temperature, chilled water temperature and cooling water temperature impose significant impacts on the water production performance of ADs based on silica gel [11,13–15]. Saha et al. [16] optimized the switching time by simulation based on silica gel-water working pairs. The results showed that too short switching time caused insufficient preheating and precooling of the adsorbent, while too long switching time caused a decrease in the number of cycles per day, both of which are detrimental to the water production performance. Youssef et al. [14,17] showed that the hot water inlet temperature, cooling water inlet temperature and condenser temperature significantly affect the SDWP and PR of the ADs. The higher SDWP and PR can be achieved under low cooling water inlet temperature, low condensing temperature and high hot water inlet temperature. The adsorption characteristics [18] (i.e.adsorption isotherms and kinetics) of adsorbents play more crucial roles. It has been reported that the larger water uptake and faster adsorption/desorption rate are beneficial for SDWP. Thus, exploring high-performing adsorbents is also an effective strategy to improve the water production performance of ADs.

Metal-organic frameworks (MOFs) consisting of metal clusters and organic ligands are porous nano-materials with ultrahigh specific surface area, large pore volume, high structure diversity and tenability [19], which endows MOFs with potential water adsorption performance for ADs. It has been reported in an experimental study that a single-bed ADs using a MOF adsorbent, CPO-27(Ni), is able to achieve a maximum SDWP of 22.8 m^3/(ton·day) at a regeneration temperature of 95 °C, evaporation temperature of 40 °C and condensation temperature of 5 °C [20]. Another mathematical modelling study of an ADs based on MOF N-UiO-66 revealed that a remarkably high SDWP of 37.6 m^3/(ton·day) can be obtained for N-UiO-66-based ADs, which is more than twice of silica gel(14.5 m^3/(ton·day)) at identical operation conditions [21]. However, silica gel outperforms MOFs at certain conditions. It has been reported in an experimental study that an ADs based on silica gel exhibited the higher SDWP of 3.2 m^3/(ton·day) than 2.6 m^3/(ton·day) of aluminium fumarate at $T_{chilled}$ = 10 °C [22]. Nevertheless, at $T_{chilled}$ = 30 °C, aluminium fumarate works better with a SDWP of 6.8 m^3/(ton·day) compared to 5 m^3/(ton·day) of silica gel. The different performance under varying working conditions may be related with the water adsorption characteristics of adsorbents.

In order to identify suitable adsorbents under varying working conditions as well as reveal the correlation between adsorption characteristics of adsorbents and desalination performance, in this work, the adsorption characteristics of 12 adsorbents including MOFs, silica gels, zeolites and polymers were collected and analyzed, based on which the performance of ADs based on MOFs and other adsorbents at different operation conditions were investigated by mathematical modeling. The top performers under specific operation conditions was identified, and the correlation between water adsorption characteristics of adsorbents and their desalination performance were eventually explored.

2. Methodology

2.1. Experiments

The synthesis of UiO-66 [23], DUT-67 [24] and MIL-101(Cr) [25] were conducted according to the previously reported protocols as

described in Supplementary Information (SI). The materials were characterized by powder X-ray diffraction (Fig. S1) to determine whether they have been successfully prepared. The water adsorption isotherms (Fig. S2) were measured by an Autosorb-iQ2 from Quantachrome Instruments at 288 K and 298 K. The water adsorption kinetics (Figs. S4-6) was captured via an intelligent dynamic vapor sorption instrument (DVS) from Surface Measurement Systems at 303 K, 313 K and 323 K.

2.2. AD system description

The schematic of the two-bed AD system consisting of an evaporator, a condenser and two adsorption beds is shown in Fig. 1. The thermodynamic cycle of ADs including pre-heating (I-II), desorption (II-III), pre-cooling (III-IV) and adsorption (IV-I) is depicted in P-T-W diagram is shown in Fig. 1b. This system has three modes: Mode A, B and C. In Mode A (Fig. 1a), valves V1 and V3 are opened, while valves V2 and V4 are closed, in which Bed 1 is in adsorption process and Bed 2 is in desorption process. In adsorption process, seawater is injected into the evaporator and evaporates at $T = T_{evap}$ and $P = P_{evap}$). The latent heat for evaporation is supplied by chilled water ($T_{chilled}$) through the heat exchanger, thus generating cooling effect. In the meanwhile, the evaporated vapor is adsorbed by Bed 1 under $T = T_{ads}$ and $P = P_{ads} = P_{evap}$, at which cooling water ($T_{cooling}$) removes the adsorption heat (Q_{ads}). In desorption process, Bed 2 is heated up to T_{des} by hot water (T_{hot}, Q_{des}), thus the regeneration of Bed 2 takes place at $T = T_{des}$ and $P = P_{des} = P_{cond}$. The desorbed vapor is condensed to produce the desalinated fresh water at $T = T_{cond}$ and $P = P_{cond}$, and the accompanying heat released from condensation is carried away by the cooling water ($T_{cooling}$). After that, Bed 1 and Bed 2 exchange their roles. The thermodynamic cycle is continued after a short switching duration (50 s) named pre-heating and pre-cooling (Mode B). In this case, all the valves are closed, and the fluid flows (hot and cooling water) are redirected to maintain the pre-heating and pre-cooling of Bed 1 and Bed 2, respectively. When the pressures of Bed 1 and Bed 2 are nearly equal to the pressures of condenser and evaporator, the valves V2 and V4 are opened, and V1 and V3 keep closed. In this case, Bed 1 is in desorption process and Bed 2 is in adsorption process, which is defined as Mode C. T_{evap} and P_{evap} (P_{ads}) are determined by $T_{chilled}$, and T_{cond} and P_{cond} (P_{des}) are determined by $T_{cooling}$ through heat exchanger. Similarly, T_{ads} depends on $T_{cooling}$, and T_{des} depends on T_{hot}.

The dynamic adsorption processes is taken into account in the numerical simulation of ADs system. The transient water loading of adsorption bed is a function of temperature, pressure and time, which is described as $W = W(T, P, t)$, and can be estimated by using the well-known LDF equation [26]:

$$\frac{dW(t)}{dt} = \frac{F_o D_{so}}{R_p^2} \exp\left(\frac{-E_a}{RT}\right)(W(\infty) - W(t))$$

where, W(t) represents transient water loading at certain conditions, $W(\infty)$ represents equilibrium water uptake, E_a and D_{so} are kinetic parameters. $W(\infty)$ can be obtained through equilibrium water adsorption isotherms, and E_a and D_{so} can be acquired from dynamic water adsorption tests. Thus, W(t) at given working conditions can be calculated according to LDF equation. The water transfer amount per cycle $\Delta W(t)$ is defined as the W(t) difference between adsorption and desorption conditions at a given cycle time, which is described as $\Delta W(t) = W(T_{ads}, P_{evap}, t) - W(T_{des}, P_{cond}, t) = W_{ads}(t) - W_{des}(t)$ shown in Fig. 1c.

2.3. Adsorption isotherm and kinetic models

In addition to the water adsorption isotherms of UiO-66, DUT-67 and MIL-101(Cr) measured in this work, experimentally measured equilibrium water adsorption isotherms of the other nine adsorbents were obtained from previous reports [27–35]. Fitting the experimentally measured water adsorption isotherms by a universal isotherm model (Eq. (1) [36]) that is applicable to all types of adsorption isotherms gives rise to the equilibrium water loading $W(\infty)$ at different temperatures. The fitting parameters (Table S1) and validity of the universal isotherm model (Fig. S3) for 12 adsorbents were provided in SI.

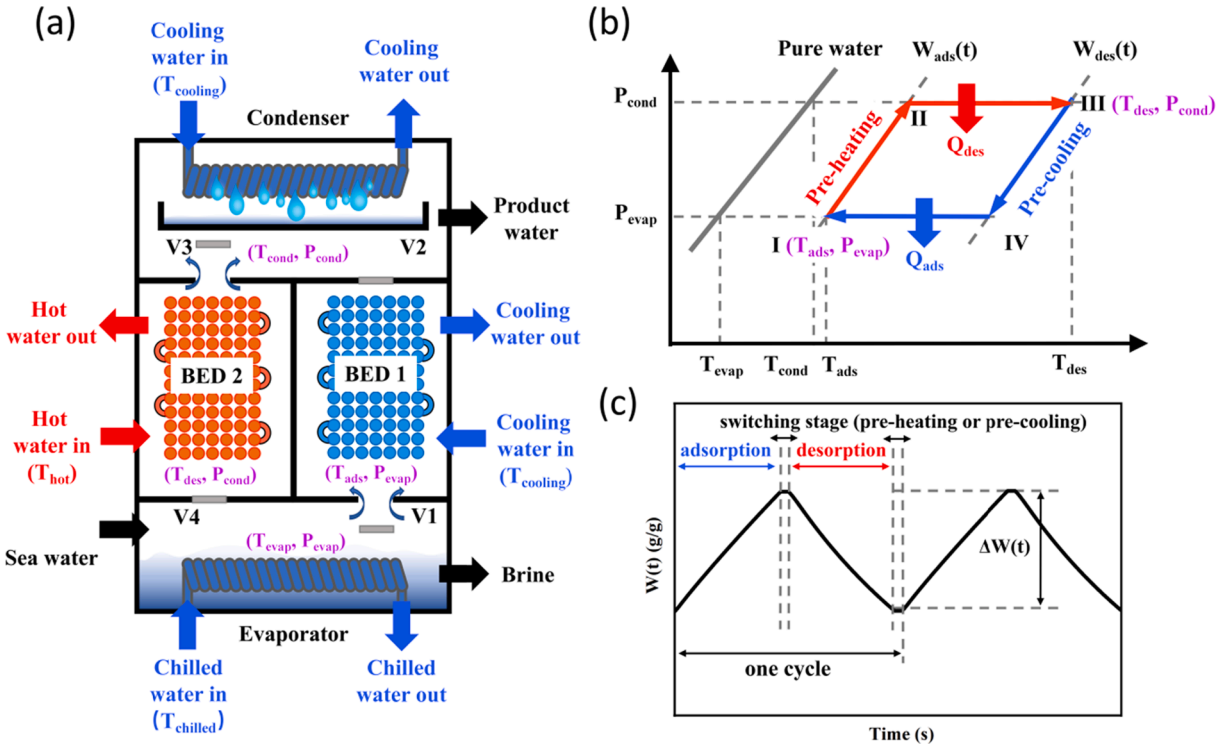

Fig. 1. (a) Schematic diagram (Mode A) and (b) thermodynamic cycle of adsorption desalination system; (c) schematic transient water loading (W(t)) and water transfer amount per cycle ($\Delta W(t)$) in ADs.

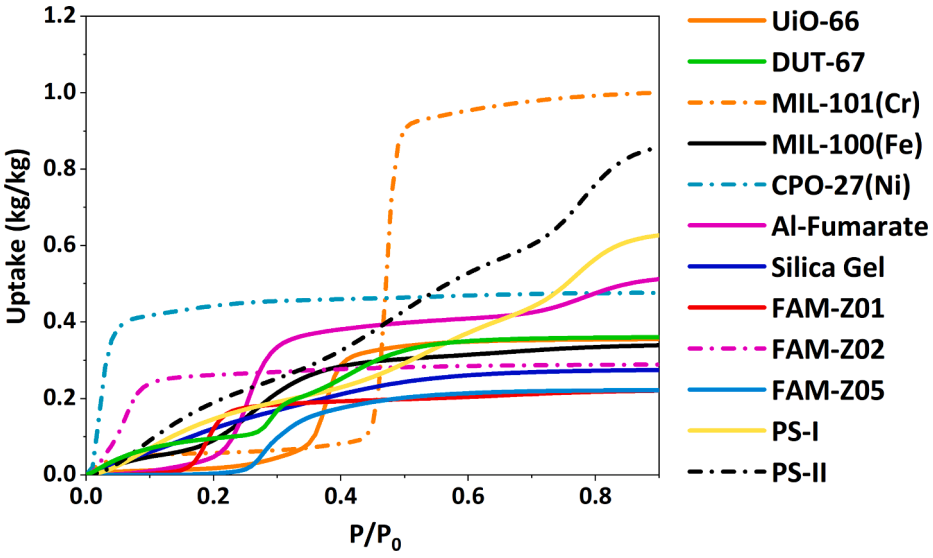

Fig. 2. Water adsorption isotherms of 12 adsorbents at T = 303 K.

$$\theta_t = \sum_{i=1}^{n} \alpha_i \left\{ \frac{\left(\frac{P}{P_s}\exp\left(\frac{\varepsilon_{oi}}{RT}\right)\right)^{\frac{RT}{m_i}}}{1+\left(\frac{P}{P_s}\exp\left(\frac{\varepsilon_{oi}}{RT}\right)\right)^{\frac{RT}{m_i}}} \right\}_i \quad (1)$$

where θ_t defines the ratio of the uptake at the specific temperature and pressure to the saturated capacity, α_i denotes the probability factor used to characterize the energy distribution of adsorption sites, ε_{oi} indicates the adsorption energy sites with maximum probability, and m_i represents the range of the energy sites available for adsorption.

The linear driving force model (LDF) is one of the most commonly used models for adsorption kinetics defined as Eq. (2) [26].

$$\frac{dW(t)}{dt} = \frac{F_o D_s}{R_p^2}(W(\infty) - W(t)) \quad (2)$$

where W(t) and W(∞) denote the transient and equilibrium water loading, F_o indicates the geometric parameter describing the shape of the adsorbent particles, D_s is the surface diffusion coefficient, R_p represents the radius of the particle. With the introduction of the fractional uptake $F = \frac{W(t)-W(0)}{W(\infty)-W(0)}$ and the dimensionless time $\theta = \frac{D_s}{R_p^2}t$, Eq. (2) can be linearized as follows:

$$\ln(1-F) = -F_o\theta = -F_o\frac{D_s}{R_p^2}t \quad (3)$$

The diffusion time constant $\frac{D_s}{R_p^2}$ at specific temperature and pressure can be obtained from the slope of Eq. (3) based on the experimental data. Since D_s is affected by temperature, the classical Arrhenius equation (Eq. (4) [34]) was developed to obtain the surface diffusion coefficient D_s at different temperatures, where E_a and D_{so} represent the activation energy and pre-exponential constant, respectively. LDF model can be eventually described by Eq. (5).

$$D_s = D_{so}\exp\left(\frac{-E_a}{RT}\right) \quad (4)$$

$$\frac{dW(t)}{dt} = \frac{F_o D_{so}}{R_p^2}\exp\left(\frac{-E_a}{RT}\right)(W(\infty) - W(t)) \quad (5)$$

The fitting parameters $\frac{F_o D_{so}}{R_p^2}$ and E_a of 12 adsorbents were presented in Table S2.

2.4. Lumped-parameter model of ADs

The lumped-parameter model of ADs including mass and energy balance of each component, was employed [8]. The model is based on the following assumptions: (1) each position of a component possesses the same physical state, (2) the adsorbed phase is assumed as the liquid phase and (3) heat loss from the system is not taken into account [26].

2.4.1. Adsorption bed

The evaporated water vapor enters into the fixed bed by the adsorption of adsorbents (affinity of adsorbents for water). The enthalpy of adsorption is removed by the cooling water through the heat exchanger. On the other hand, the hot water is supplied to meet the requirement of desorption heat, and the desorbed water vapor is subsequently transferred into the condenser. The energy exchange in the bed includes sensible heat caused by temperature change, adsorption heat due to mass transfer and the heat exchanged between cooling/hot water and the bed. Hence, the energy balance is given by

$$\frac{dT_{bed,i}}{dt}\left(\left(Mc_p\right)_{hx,bed} + \left(Mc_p\right)_{ad} + M_{ad}W(t)c_{p,v}\right) = \phi M_{ad}\frac{dW_i(t)}{dt}Q_{st} + \left(mc_p\right)_j(T_{in} - T_{out})_j \quad (6)$$

where $(Mc_p)_{hx,bed} + (Mc_p)_{ad} + M_{ad}W(t)c_{p,v}$ gives the heat capacity of heat exchanger, adsorbents and adsorbed water vapor. The left hand side of Eq. (6) is related to the sensible heat caused by temperature variation in the bed. $M_{ad}\frac{dW_i(t)}{dt}Q_{st}$ represents the enthalpy of adsorption/desorption, and $(mc_p)_j(T_{in} - T_{out})_j$ indicates the heat exchanged between cooling/hot water and the bed through heat exchanger, where mc_p is the heat capacity of water. The flag $\phi = 1$ represents the adsorption/desorption process while $\phi = 0$ represents the switching duration, i refers to adsorption or desorption state, and j represents cooling (adsorption process) or hot water (desorption process).

2.4.2. Evaporator

The charging seawater is continuously fed into the evaporator, and evaporates with latent heat supplied by the chilled water through the heat exchanger. Then, the evaporated water vapor is adsorbed by the adsorbents, and the concentrated brine discharges from the evaporator. The energy balance of evaporator becomes

$$\frac{dT_{evap}}{dt}\left(\left(Mc_p\right)_{hx,evap}+M_{s,evap}c_{p,s}\right) = m_{s,in}h_{f,s}-m_bh_{f,b}-M_{ad}\frac{dW_{ads}(t)}{dt}h_{fg}+\left(mc_p\right)_{chilled}\left(T_{in}-T_{out}\right)_{chilled} \quad (7)$$

where $M_{s,evap}$ defines the amount of seawater in the evaporator, and $m_{s,in}$ and m_b represent the mass rate of feed seawater and brine discharged from the evaporator respectively. The left hand side of Eq. (7) displays the sensible heat variation of the evaporator including the contributions from the heat exchanger and seawater. $m_{s,in}h_{f,s}$ and $m_bh_{f,b}$ stands for the sensible heat carried by the feed seawater and removal by the brine discharge. $M_{ad}\frac{dW_{ads}(t)}{dt}h_{fg}$ denotes latent heat caused by evaporation, and $(mc_p)_{chilled}(T_{in}-T_{out})_{chilled}$ indicates the energy provided by the chilled water. The mass variation in the evaporator becomes

$$\frac{dM_{s,evap}}{dt} = m_{s,in}-m_b-M_{ad}\frac{dW_{ads}(t)}{dt} \quad (8)$$

2.4.3. Condenser

The desorbed vapor is condensed in the condenser with the accompanying heat of condensation being carried away by the cooling water through the heat exchanger. Thus, the energy balance is given by

$$\frac{dT_{cond}}{dt}\left(\left(Mc_p\right)_{hx,cond}+M_{w,cond}c_{p,w}\right) = \phi M_{ad}\frac{dW_{des}(t)}{dt}h_{fg}+M_{ad}\frac{dW_{des}(t)}{dt}c_{p,v}\left(T_{bed}-T_{cond}\right)+\left(mc_p\right)_{cooling}\left(T_{in}-T_{out}\right)_{cooling}-m_dh_{f,d} \quad (9)$$

where $(Mc_p)_{hx,cond}+M_{w,cond}c_{p,w}$ stands for the heat capacity of heat exchanger and the desalinated water retained in the condenser. $M_{ad}\frac{dW_{des}(t)}{dt}h_{fg}$ defines the condensation heat of the desorbed water vapor. $M_{ad}\frac{dW_{des}(t)}{dt}c_{p,v}(T_{bed}-T_{cond})$ represents the sensible heat of the inlet desorbed water vapor. $(mc_p)_{cooling}(T_{in}-T_{out})_{cooling}$ relates the energy carried away by the cooling water through the heat exchanger. $m_dh_{f,d}$ is the amount of sensible heat removal by the discharge of desalinated water.

Table 1
Key physical parameters in the model [38].

Symbol	Description	Value	Unit
M_{ad}	Mass of adsorbent	6.75	kg
$M_{s,evap}$	seawater in side evaporator initially	3	kg
$(Mc_p)_{hx,bed}$	Thermal mass of bed	1798	J/K
$(Mc_p)_{hx,evap}$	Thermal mass of evaporator	501.8	J/K
$(Mc_p)_{hx,cond}$	Thermal mass of condenser	592.5	J/K
UA_{bed}	Overall heat transfer coefficient of bed	600	W/K
UA_{evap}	Overall heat transfer coefficient of evaporator	350	W/K
UA_{cond}	Overall heat transfer coefficient of condenser	500	W/K
m_{hot}	Hot water flow rate	0.2	kg/s
$m_{chilled}$	Chilled water flow rate	0.025	kg/s
$m_{cooling}$	Cooling water flow rate	0.3	kg/s
$c_{p,ad}$	Adsorbent specific heat	1×10^3	J/(kg·K)
$c_{p,w}$	Water specific heat	4.18×10^3	J/(kg·K)
$c_{p,v}$	Vapor specific heat	1.89×10^3	J/(kg·K)
T_{hot}	Hot water inlet temperature	60–90	°C
$T_{chilled}$	Chilled water inlet temperature	10–30	°C
$T_{cooling}$	Cooling water inlet temperature	30	°C

Similar to the evaporator, the mass variation in the condenser becomes

$$\frac{dM_{w,cond}}{dt} = M_{ad}\frac{dW_{des}(t)}{dt}-m_d \quad (10)$$

where $\frac{dM_{w,cond}}{dt}$ represents the mass variation of condensed water, $M_{ad}\frac{dW_{des}(t)}{dt}$ stands for the desorbed vapor transferred to the condenser and m_d denotes the fresh water discharged.

2.4.4. Heat exchanger

The outlet water temperature of all heat exchangers including adsorption beds, evaporator and condenser, is calculated by the logarithmic mean temperature difference (LMTD) method, which is expressed as

$$T_{out} = T_{hx}+(T_{in}-T_{hx})\exp\left(\frac{-(UA)_{hx}}{mc_p}\right) \quad (11)$$

where T_{in} and T_{out} stand for the inlet and outlet temperature of hot/chilled/cooling water, and T_{hx} stands for the temperature of the heat exchanger. $(UA)_{hx}$ is the overall heat transfer coefficient of the heat exchanger which is provided in Table 1.

2.4.5. Performance index

For assessment of the ADs performance, indexes including specific daily water production (SDWP) and performance ratio (PR) were calculated according to Eq. (12) and Eq. (13). SDWP (m^3/(ton·day)) is the amount of fresh water produced by one ton of adsorbent per day. PR is the energy utilization efficiency of the ADs, which equals to the condensation heat of desorbed vapor divided by the heat input to the system.

$$SDWP = \tau\int_0^{t_{cycle}}dW(t)dt = \tau\int_0^{t_{cycle}}\frac{(mc_p)_{cooling}(T_{out}-T_{in})_{cooling}}{h_{fg}M_{ad}}dt \quad (12)$$

$$PR = \frac{h_{fg}\int_0^{t_{cycle}}dW(t)dt}{\int_0^{t_{cycle}}(mc_p)_{hot}(T_{in}-T_{out})_{hot}dt} \quad (13)$$

where τ in Eq. (12) denotes the number of cycles per day. In this work, T_{hot} varies from 60 to 90 °C, $T_{chilled}$ is 10, 20 and 30 °C respectively, $T_{cooling}$ is 30 °C and half cycle time is 700 s. Based on experimentally measured adsorption kinetics, ADs were modeled using MATLAB software with the differential equations numerically solved by an ODE45 solver after the initial values were assumed. The relative error of the solver was set to 0.001 [37] (convergent criterion). The model was based on the same physical parameters (Table 1) from literature [38] to ensure the validity and reliability (Fig. S7), which has been validated in previous study [38].

3. Results and discussion

3.1. Adsorption isotherms

The water adsorption isotherms of 12 adsorbents are classified according to the IUPAC [39]. Different shapes of water adsorption isotherms are related to their structure properties. CPO-27(Ni) exhibited type I adsorption isotherm with a maximum water uptake of 0.47 g/g, which can be ascribed to its dominant micropore size of 1.2 nm [40] that

favors the strong interaction between water molecules and unsaturated metal centres (UMCs) in CPO-27(Ni) [40]. However, too strong affinity towards water molecules requires a high desorption temperature which may be detrimental to PR due to the fact that a larger amount of energy input is consumed to desorb water from adsorbents. Different from porous materials, water molecules are mainly adsorbed onto the outer surface of the polymers initially [34], and then diffuse into polymeric chains with multilayer adsorption, at which the polymer swells. Both PS-I and PS-II displayed type II isotherms with very low pore volume and the maximum water uptake of 0.62 g/g and 0.85 g/g, respectively. The rest adsorbents show "S-shaped" or type V isotherm with different adsorption steps. FAM (aluminophosphate based) zeolites are potential adsorbents for adsorption cooling and dehumidification [31,41]. Zeolite FAM-Z01 is consisted of AlO_4, PO_4 and FeO_4 tetrahedron with Al and P atoms partially replaced by Fe atoms, which exhibits a BET surface area of 189.6 m^2/g and pore volume of 0.071 cm^3/g [33]. Similar to FAM-Z01, FAM-Z05 consisting of only AlO_4 and PO_4 tetrahedrons possessed the BET surface area of 187.1 m^2/g and pore volume of 0.07 cm^3/g [33]. The Fe atoms of FAM-Z01 is more attractive to water molecules due to the higher enthalpies of adsorption. Therefore, FAM-Z01 shows shorter hydrophobic length of $P/P_0 = 0.15$ compared to $P/P_0 = 0.25$ of FAM-Z05. The hydrophobic length is the relative pressure P/P_0 at which the sudden rise in water uptake is observed. However, their saturation water uptake of 0.22 g/g is comparable due their similar pore volumes. FAM-Z02 is a silico-aluminophosphate consisting of AlO_4, PO_4 and SiO_4 tetrahedrons with a BET surface area of 717.8 m^2/g and pore volume of 0.27 cm^3/g [33]. In the presence of SiO_4, FAM-Z02 shows a very short hydrophobic length of $P/P_0 = 0.05$ and the higher water uptake of 0.28 g/g due to its larger surface area and pore volume.

Compared to conventional silica gels and zeolites, MOF-based adsorbents show relatively higher saturation uptake. Mesoporous MIL-101 (Cr) has been widely investigated due to its ultra-high BET surface area of 3358 m^2/g and pore volume of 2.09 cm^3/g [42]. The initial low water uptake at relative pressure of $P/P_0 < 0.4$ is usually ascribed to the possible chemisorption on unsaturated metal sites [43]. The steep water adsorption step at $P/P_0 = 0.45$ indicates the pore filling of the cages in MIL-101(Cr). Due to the largest pore volume, MIL-101(Cr) achieved the highest water uptake of 1.01 g/g at $P/P_0 = 0.9$ among 12 adsorbents, which is 274.1% and 248.2% higher than silica gel and FAM-Z02, respectively. Unfortunately, its long hydrophobic length of $P/P_0 = 0.45$ may restrict the water production performance. MIL-100(Fe) contains smaller mesoporous cages than MIL-101(Cr), which shifts the adsorption step to $P/P_0 \approx 0.3$ and gives rise to a smaller water uptake of 0.34 g/g which is still 25.9% and 17.2% higher than silica gel and FAM-Z02, respectively. Two Zr-based MOFs, DUT-67 and UiO-66, were investigated due to their high water stability [44]. DUT-67 is a microporous MOF with a surface area of 1064 m^2/g, pore volume of 0.44 cm^3/g and pore size of 1.17/1.42 nm [24], and it shows a desired "S-shaped" water adsorption isotherm with three steps locating within $P/P_0 = 0.1–0.4$. The neutron powder diffraction test on the D_2O-loaded DUT-67 indicated that these three adsorption steps are related to the pore filling starting from the smallest pore to the middle and largest pores [45]. UiO-66 is also a microporous MOF with a surface area of 1508 m^2/g, pore volume of 0.99 cm^3/g and pore size of 1.06 nm [46]. However, UiO-66 shows a longer hydrophobic length of $P/P_0 = 0.35$ than DUT-67 due to the hydrophobicity of the phenol rings of its ligand. The pore filling in

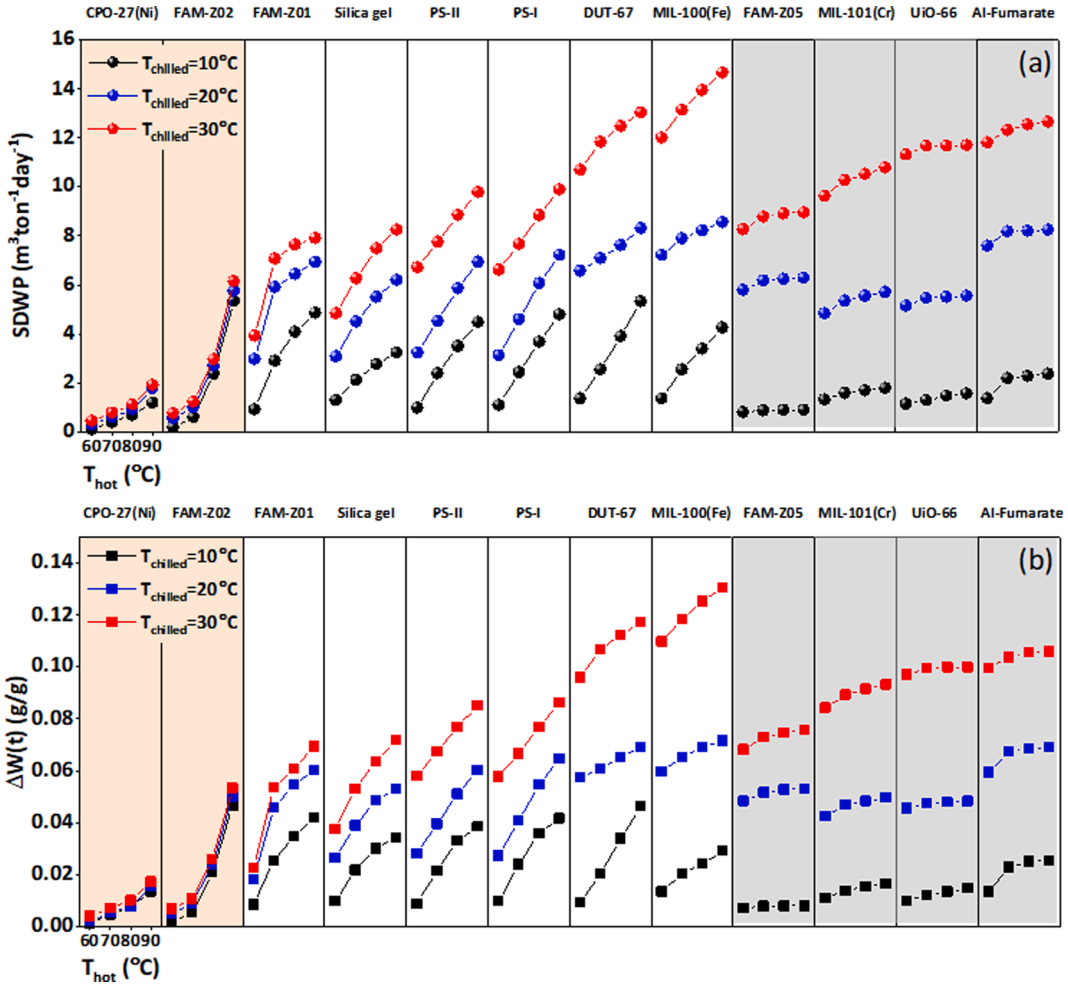

Fig. 3. (a) SDWP and (b) ΔW(t) of the ADs based on 12 adsorbents at T_{hot} = 60, 70, 80 and 90 °C and $T_{chilled}$ = 10, 20 and 30 °C, respectively.

UiO-66 occurs at $0.3 < P/P_0 < 0.4$ and the maximum water uptake is around 0.36 g/g, which is 33.3% and 24.1% higher than silica gel and FAM-Z02.

3.2. Water production performance

According to numerical simulations, SDWP of ADs based on various adsorbents under different T_{hot} and $T_{chilled}$ were investigated (Fig. 3a). It is found that SDWP generally increases with T_{hot}, which is due to the more complete desorption at higher T_{hot}. Nevertheless, SDWP of FAM-Z05, MIL-101(Cr), UiO-66 and aluminium fumarate is slightly affected by T_{hot} (highlighted by gray region in Fig. 3a) at a constant $T_{chilled}$. In contrast, a remarkable increase of SDWP with T_{hot} is observed for CPO-27(Ni), FAM-Z02, FAM-Z01, silica gel, PS-II, PS-I, DUT-67 and MIL-100 (Fe). Such tendencies are well correlated with their water transfer amount per cycle ΔW(t) shown in Fig. 3b, since SDWP is determined by ΔW(t) of each adsorbent according to Eq. (12). On the other hand, SDWP increases with $T_{chilled}$ which is ascribed to the higher ΔW(t) resulting from the enhanced adsorption pressure (P_{ads}) under higher $T_{chilled}$. The remarkable improvement of SDWP is found for DUT-67, MIL-100(Fe), FAM-Z05, MIL-101(Cr), UiO-66 and aluminium fumarate as $T_{chilled}$ increased from 10 °C to 30 °C, and moderate improvement of SDWP is found for silica gel, PS-I and PS-II. However, CPO-27(Ni) and FAM-Z02 exhibit independence of $T_{chilled}$ (orange region in Fig. 3a), which is also correlated with their water transfer amount per cycle ΔW(t)(Fig. 3b). Although the strong correlation between SDWP and ΔW(t) is demonstrated in Fig. 3, the underlying relationship between adsorption characteristics of adsorbents and ΔW(t), which is essential for choosing and design of high-performing adsorbents for ADs, has yet to be elucidated.

In order to disclose such a relationship between ΔW(t) and adsorption characteristics of adsorbents, representative adsorbents FAM-Z02, PS-I and UiO-66 exhibiting different trends in ΔW(t) with T_{hot} and $T_{chilled}$ were selected(Fig. 4). Since the variation in W(t) during a single adsorption–desorption cycle corresponds to ΔW(t), W(t) of typical

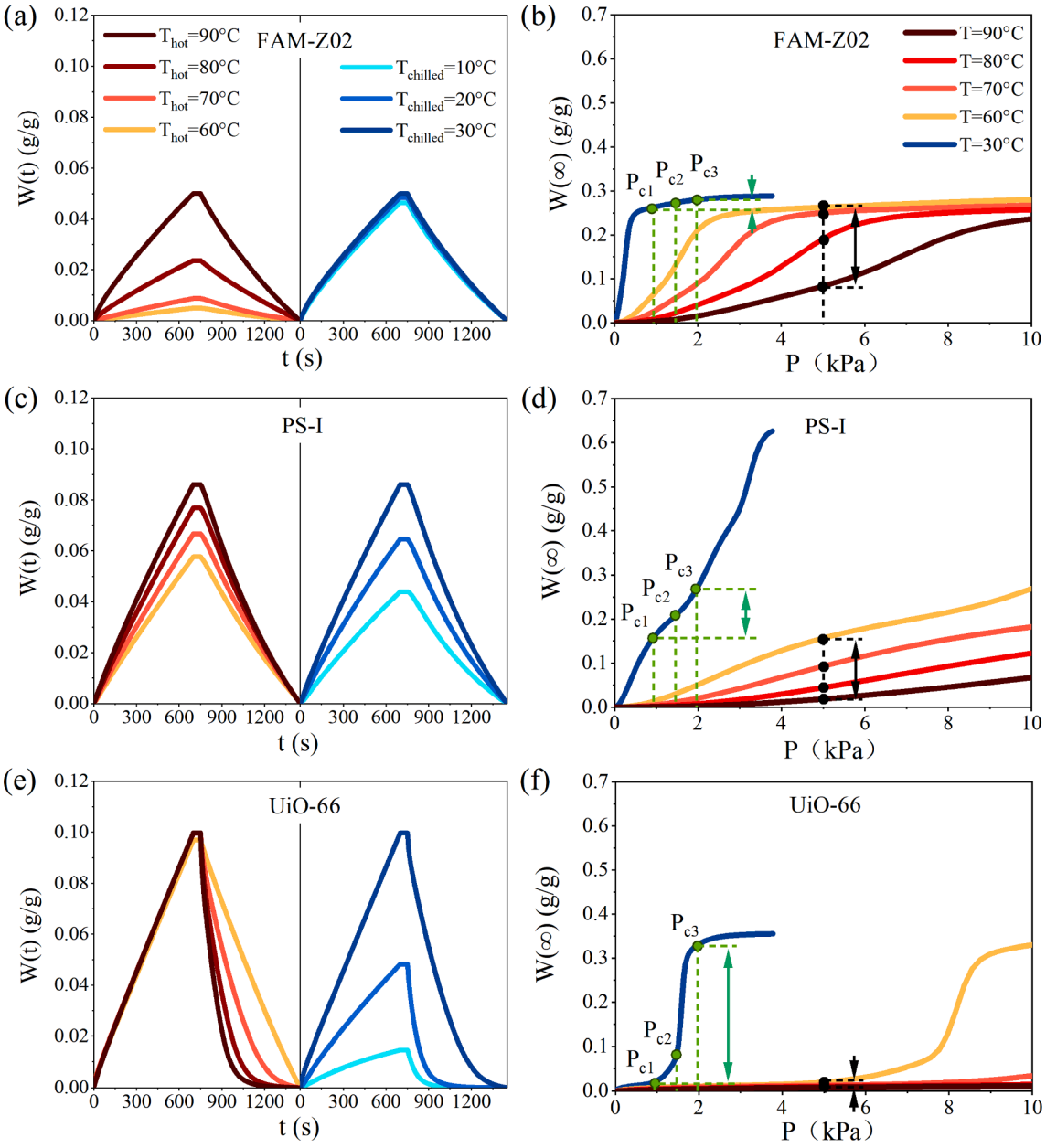

Fig. 4. Effects of T_{hot} and $T_{chilled}$ on transient water loading W(t) and water adsorption isotherms based on adsorbents possessing type I(FAM-Z02), type II(PS-I) and type "S-shaped"(UiO-66) isotherms. The subscript c1, c2 and c3 represent the cases under $T_{chilled}$ = 10, 20 and 30 °C.

adsorbents were analyzed. It is found that W(t) of adsorbents with type I isotherms (e.g.FAM-Z02) or strong hydrophilicity is highly sensitive to T_{hot} but less sensitive to $T_{chilled}$, leading to remarkable increase of ΔW(t) with T_{hot} and unnoticeable variation of ΔW(t) with $T_{chilled}$(Fig. 4a). This is because the increase of T_{hot} significantly affects the equilibrium water uptake W(∞) of adsorbents with type I isotherms at identical pressure, whereas the increase of $T_{chilled}$ changes the adsorption pressures that correspond to slight variation in water uptake of type I isotherms (Fig. 4b). Similarly, adsorbents with type II isotherms (e.g. PS-I), W(t) is sensitive to both T_{hot} and $T_{chilled}$, resulting in the significantly increased ΔW(t) with T_{hot} and $T_{chilled}$(Fig. 4c), which is because the increase of T_{hot} and $T_{chilled}$ imposes remarkable increase in equilibrium water uptake W(∞)(Fig. 4d). Considering the relationship between transient water loading W(t) and equilibrium water uptake W(∞) based on Eq. (2): $W(t)-W(0) = (W(\infty)-W(0))*(1-\exp(-\frac{F_o D_s}{R_p^2})t)$, the higher W(∞), the higher W(t) for the given adsorbent.Compared with adsorbents with type I and II isotherms, adsorbents with type V or S-shaped isotherms(e.g. UiO-66) are most favorable, since ΔW(t) is almost not changed when T_{hot} increases from 60 to 90 °C (Fig. 4e). Such a phenomenon suggests that T_{hot} = 60 °C or low-temperature heat source is sufficient for the complete desorption of water, which is beneficial for the improvement of energy efficiency or PR of ADs. On the contrary, ΔW(t) of UiO-66 is dramatically increased with $T_{chilled}$ due to its stepwise adsorption isotherm(Fig. 4f). According to Fig. 2, the adsorbents with short hydrophobic length tend to exhibit type I adsorption isotherms, the adsorbents with moderate hydrophobic length tend to exhibit type II adsorption isotherms, and the ones with long hydrophobic length tend to display type V isotherms. Such adsorption characteristics are closely correlated with SDWP under varying T_{hot} and $T_{chilled}$. In summary, SDWP of the adsorbents with strong hydrophilicity is greatly dependent on T_{hot} , whereas SDWP of the adsorbents with strong hydrophobicity mostly relies on $T_{chilled}$.

In terms of the energy utilization efficiency of ADs, the performance ratio (PR) under varying T_{hot} and $T_{chilled}$ was analyzed (Fig. 5). According to Eq. (13), PR is equal to the condensation heat of desalinated vapor $\Delta W(t)h_{fg}$ divided by the heat input to the system Q_{des}, which can be described as $PR \propto \frac{\Delta W(t)h_{fg}}{Q_{des}}$. It is found that PR of adsorbents such as CPO-27(Ni) and FAM-Z02 dramatically increases with T_{hot} due to the fact that the increase in ΔW(t) compensates for the increase in the heat Q_{des} consumed by the ADs, thus gives rise to the increased PR. Whereas PR is not evidently increased with $T_{chilled}$ since ΔW(t) is slightly affected by $T_{chilled}$ according to Fig. 4b. Nevertheless, as for FAM-Z05, MIL-101(Cr), UiO-66 and aluminium fumarate, ΔW(t) remains nearly unchanged with T_{hot} due to the complete desorption resulting from S-shaped isotherms (Fig. 4e), while the excessive heat input to the system results in a decreased PR regardless of $T_{chilled}$, implicating an increase in heat losses as the adsorption beds repeatedly switch between adsorption and desorption states. Similarly, taking into account the trade-off between ΔW(t) and Q_{des}, PR for FAM-Z01, silica gel, PS-I, PS-II, DUT-67 and MIL-100(Fe) increases with T_{hot} at $T_{chilled}$ = 10 °C and 20 °C(only for PS-I and PS-II), but decreases with T_{hot} at $T_{chilled}$ = 30 °C.

Considering both SDWP and PR of ADs under various operating conditions, the water production performance of ADs based on 12 adsorbents is summarized in Fig. 6. It is found that at $T_{chilled}$ = 10 °C, DUT-67, FAM-Z01 and PS-I are the top three performers with average SDWP = 3.31, 3.20 and 2.98 m^3/(ton·day). At $T_{chilled}$ = 20 and 30 °C, ADs based on MOFs exhibit remarkably higher performance than the ones based on other adsorbents. Among the MOFs, aluminium fumarate, MIL-100(Fe) and DUT-67 showed exceptional water production performance with 68.2%, 65.7% and 54.3% increase in average SDWP compared to silica gel at $T_{chilled}$ = 20 °C. At $T_{chilled}$ = 30 °C, MIL-100(Fe) achieved the highest average SDWP of 13.46 m^3/(ton·day) followed by DUT-67, aluminium fumarate, UiO-66 and MIL-101(Cr) with average SDWP of 12.88, 12.29, 11.64 and 10.33 m^3/(ton·day), respectively. The selected top three performers for ADs under different chilled water temperatures were summarized in Table 2. It can be found that DUT-67 is the most versatile candidate that is applicable to various working conditions, followed by MIL-100(Fe) and Al-fumarate. These findings highlight the great potential of MOFs for adsorption desalination.

DUT-67 achieved exceptional average specific daily water production (SDWP) of 3.31 m^3/(ton·day) and performance ratio (PR) of 0.33 among 12 adsorbents at the chilled water temperature of 10 °C. Aluminium fumarate outperforms other adsorbents at the chilled water temperature of 20 °C with a SDWP increased by 68.2% compared to silica gel. MIL-100(Fe) based MOFs exhibited the greatest water production performance at the chilled water temperature of 30 °C. The ΔW(t) of adsorbents with type I isotherms is significantly affected by hot water temperature, whereas the "S-shaped" one is very slightly affected. The chilled water temperature, on the other hand, imposes remarkable impacts on the ΔW(t) of "S-shaped" isotherm adsorbents, while it has slight effects on type I. This work elucidates the correlation between the water adsorption characteristics of adsorbents and the desalination performance, which provides insights into quickly choosing proper adsorbents under different operating scenarios in practical applications. Moreover, the top performers for ADs were identified from silica gels, zeolites, polymers and metal–organic frameworks through mathematical simulation, which will offer guidance for the development of high-performing ADs. This work may also inspire increasing research interests on the exploration of high-performing adsorbents by efficient theoretical evaluations.

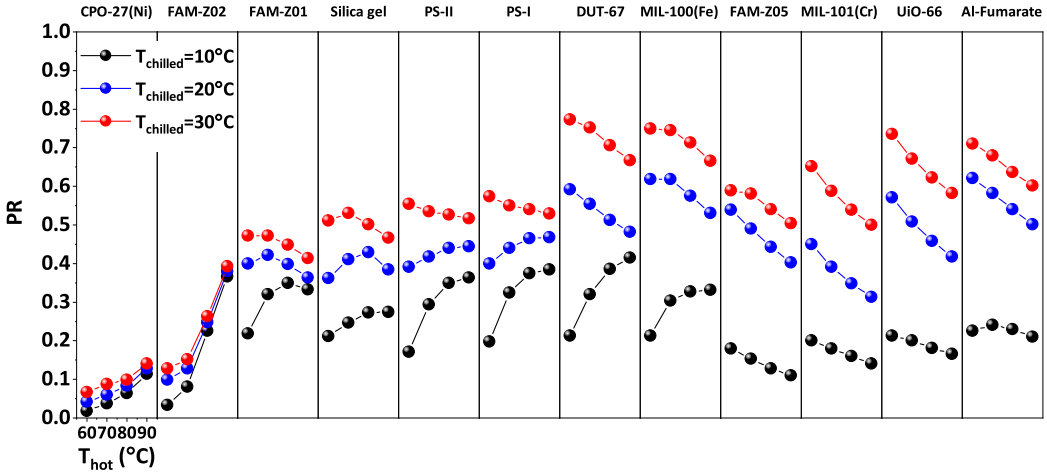

Fig. 5. The PR of ADs based on 12 adsorbents at T_{hot} varying from 60 °C to 90 °C and $T_{chilled}$ kept at 10, 20 and 30 °C respectively.

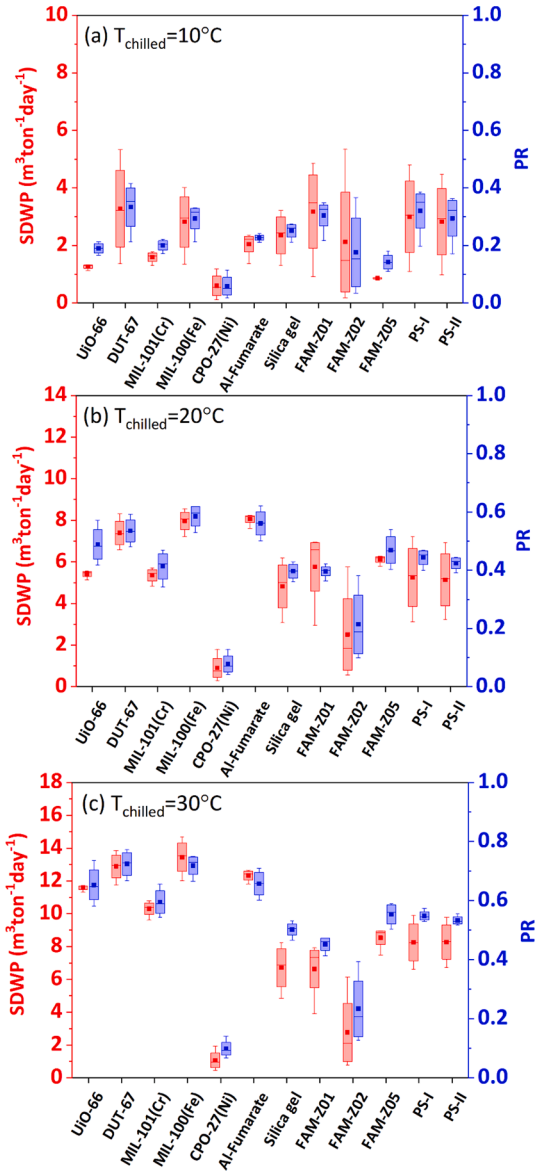

Fig. 6. The SDWP and PR distribution of 12 adsorbents at the chilled water temperature of (a) 10 °C, (b) 20 °C and (c) 30 °C, in which the mean (the line in the rectangular box), average (small squared symbols in the rectangular box), and interquartile ranges were included. The bottom and upper fences of the rectangular box represent the first and third quartiles of the data set, respectively.

Table 2
Selected top three adsorbents for ADs under various working conditions.

Application	Adsorbent		
$T_{chilled}$ = 10 °C	DUT-67	FAM-Z01	PS-I
$T_{chilled}$ = 20 °C	Al-fumarate	MIL-100(Fe)	DUT-67
$T_{chilled}$ = 30 °C	MIL-100(Fe)	DUT-67	Al-fumarate

4. Conclusion

In this work, the performance of ADs based on MOFs and other adsorbents was evaluated under various hot and chilled water temperatures. The correlation between the water adsorption characteristics of adsorbents and the desalination performance was investigated, and the top three candidates were screened under varying scenarios. It is found that SDWP dominated by the water transfer amount per cycle ΔW(t) is closely related to the shape of adsorption isotherms. Adsorbents with stepwise isotherms are preferred for ADs driven by low-grade heat sources. Taking into account both SDWP and PR, the ADs based on MOFs outperform the ones based on conventional adsorbents, and DUT-67, MIL-100(Fe) and Al-fumarate are the top three performers. Besides, DUT-67 is the most versatile candidates with outstanding performance at $T_{chilled}$ = 10, 20 and 30 °C, followed by MIL-100(Fe) and Al-fumarate. The computational approach of identifying adsorbents with outstanding desalination performance in this work is favorable for the development of high-performing ADs. The correlation between desalination performance and water adsorption characteristics of adsorbents reported in this work is not only favorable for adsorbent selection but also helpful for adsorbents design for high-efficient ADs. Moreover, because this work is only focused on the desalination performance of a limited number of MOFs, more adsorbents should be included to obtain more universal correlation, which will be taken into account in future work. In addition, minimizing heat and mass transfer resistances between adsorber and heat exchanger is a prerequisite for the enhancement of the desalination performance and the design of compact ADs units. Therefore, more efforts should be devoted to this aspect such as MOF shaping, improvement of MOF adsorption kinetics and optimization of adsorber structure.

Declaration of Competing Interest

The authors declare that they have no known competing financial interests or personal relationships that could have appeared to influence the work reported in this paper.

Data availability

Data will be made available on request.

Acknowledgements

This work was supported by National Key Research and Development Program of China (No. 2020YFB1506300). The computation was carried out at National Supercomputer Center in Shenzhen.

We thank the support from Analytical & Testing Center of Huazhong University of Science and Technology.

Appendix A. Supplementary material

Supplementary data to this article can be found online at https://doi.org/10.1016/j.applthermaleng.2022.119000.

References

[1] K.C. Ng, K. Thu, S.J. Oh, L.i. Ang, M.W. Shahzad, A.B. Ismail, Recent developments in thermally-driven seawater desalination: energy efficiency improvement by hybridization of the MED and AD cycles, Desalination 356 (2015) 255–270.
[2] J. Eliasson, The rising pressure of global water shortages, Nature 517 (7532) (2015) 6.
[3] S. Burn, M. Hoang, D. Zarzo, F. Olewniak, E. Campos, B. Bolto, O. Barron, Desalination techniques — a review of the opportunities for desalination in agriculture, Desalination 364 (2015) 2–16.
[4] O. Alnajdi, Y. Wu, J. Kaiser Calautit, Toward a sustainable decentralized water supply: review of adsorption desorption desalination (ADD) and current technologies: Saudi Arabia (SA) as a case study, Water 12 (4) (2020) 1111.
[5] M.W. Shahzad, M. Burhan, L. Ang, K.C. Ng, Energy-water-environment nexus underpinning future desalination sustainability, Desalination 413 (2017) 52–64.
[6] C. Olkis, S. Brandani, G. Santori, Cycle and performance analysis of a small-scale adsorption heat transformer for desalination and cooling applications, Chem. Eng. J. 378 (2019) 122104, https://doi.org/10.1016/j.cej.2019.122104.
[7] V.C. Panagiotopoulou, P. Stavropoulos, G. Chryssolouris, A critical review on the environmental impact of manufacturing: a holistic perspective, Int. J. Adv. Manuf. Technol. 118 (1-2) (2022) 603–625.
[8] K.C. Ng, K. Thu, Y. Kim, A. Chakraborty, G. Amy, Adsorption desalination: An emerging low-cost thermal desalination method, Desalination 308 (2013) 161–179.

[9] S.-Y. Woo, H.-S. Lee, H.o. Ji, D.-S. Moon, Y.-D. Kim, Silica gel-based adsorption cooling cum desalination system: focus on brine salinity, operating pressure, and its effect on performance, Desalination 467 (2019) 136–146.
[10] K. Thu, B.B. Saha, S. Mitra, K.J. Chua, Modeling and simulation of mass recovery process in adsorption system for cooling and desalination, Energy Procedia 105 (2017) 2004–2009.
[11] K. Thu, K.C. Ng, B.B. Saha, A. Chakraborty, S. Koyama, Operational strategy of adsorption desalination systems, Int. J. Heat Mass Transf. 52 (7-8) (2009) 1811–1816.
[12] K. Thu, A. Chakraborty, Y.-D. Kim, A. Myat, B.B. Saha, K.C. Ng, Numerical simulation and performance investigation of an advanced adsorption desalination cycle, Desalination 308 (2013) 209–218.
[13] X. Wang, K.C. Ng, Experimental investigation of an adsorption desalination plant using low-temperature waste heat, Appl. Therm. Eng. 25 (17-18) (2005) 2780–2789.
[14] P.G. Youssef, R.K. AL-Dadah, S.M. Mahmoud, H.J. Dakkama, A. Elsayed, Effect of evaporator and condenser temperatures on the performance of adsorption desalination cooling cycle, Energy Procedia 75 (2015) 1464–1469.
[15] K.C. Ng, K. Thu, B.B. Saha, A. Chakraborty, Study on a waste heat-driven adsorption cooling cum desalination cycle, Int. J. Refrig 35 (3) (2012) 685–693.
[16] I.I. El-Sharkawy, H. AbdelMeguid, B.B. Saha, Towards an optimal performance of adsorption chillers: reallocation of adsorption/desorption cycle times, Int. J. Heat Mass Transf. 63 (2013) 171–182.
[17] R. Raj, V. Baiju, Thermodynamic analysis of a solar powered adsorption cooling and desalination system, Energy Procedia 158 (2019) 885–891.
[18] A.R. Lucaci, D. Bulgariu, I. Ahmad, G. Lisă, A.M. Mocanu, L. Bulgariu, Potential use of biochar from various waste biomass as biosorbent in Co (II) removal processes, Water 11 (8) (2019) 1565, https://doi.org/10.3390/w11081565.
[19] T.R. Cook, Y.-R. Zheng, P.J. Stang, Metal-organic frameworks and self-assembled supramolecular coordination complexes: comparing and contrasting the design, synthesis, and functionality of metal-organic materials, Chem Rev 113 (1) (2013) 734–777.
[20] P.G. Youssef, H. Dakkama, S.M. Mahmoud, R.K. AL-Dadah, Experimental investigation of adsorption water desalination/cooling system using CPO-27Ni MOF, Desalination 404 (2017) 192–199.
[21] B.o. Han, A. Chakraborty, Advanced cooling heat pump and desalination employing functional UiO-66 (Zr) metal-organic frameworks, Energy Convers. Manage. 213 (2020) 112825, https://doi.org/10.1016/j.enconman.2020.112825.
[22] E. Elsayed, R. AL-Dadah, S. Mahmoud, P. Anderson, A. Elsayed, Experimental testing of aluminium fumarate MOF for adsorption desalination, Desalination 475 (2020) 114170, https://doi.org/10.1016/j.desal.2019.114170.
[23] A. Schaate, P. Roy, A. Godt, J. Lippke, F. Waltz, M. Wiebcke, P. Behrens, Modulated synthesis of Zr-based metal-organic frameworks: from nano to single crystals, Chemistry 17 (24) (2011) 6643–6651.
[24] V. Bon, I. Senkovska, I.A. Baburin, S. Kaskel, Zr- and Hf-based metal-organic frameworks: tracking down the polymorphism, Cryst. Growth Des. 13 (3) (2013) 1231–1237.
[25] P.B.S. Rallapalli, M.C. Raj, S. Senthilkumar, R.S. Somani, H.C. Bajaj, HF-free synthesis of MIL-101(Cr) and its hydrogen adsorption studies, Environ. Prog. Sustainable Energy 35 (2) (2016) 461–468.
[26] E. Elsayed, R. Al-Dadah, S. Mahmoud, et al., Adsorption cooling system employing novel MIL-101(Cr)/CaCl2 composites: numerical study, Int. J. Refrig 107 (2019) 246–261.
[27] A. Rezk, R. Al-Dadah, S. Mahmoud, et al., Characterisation of metal organic frameworks for adsorption cooling, Int. J. Heat Mass Transf. 55 (25–26) (2012) 7366–7374.
[28] N. ul Qadir, S.A.M. Said, R.B. Mansour, Performance prediction of a two-bed solar adsorption chiller with adaptive cycle time using a MIL-100(Fe)/water working pair – influence of solar collector configuration, Int. J. Refrig. 85 (2018) 472–488.
[29] E. Elsayed, R. Al-Dadah, S. Mahmoud, et al., Aluminium fumarate and CPO-27(Ni) MOFs: Characterization and thermodynamic analysis for adsorption heat pump applications, Appl. Therm. Eng. 99 (2016) 802–812.
[30] K. Thu, H. Yanagi, B.B. Saha, et al., Performance investigation on a 4-bed adsorption desalination cycle with internal heat recovery scheme, Desalination 402 (2017) 88–96.
[31] S.W. Hong, S.H. Ahn, J.D. Chung, et al., Characteristics of FAM-Z01 compared to silica gels in the performance of an adsorption bed, Appl. Therm. Eng. 104 (2016) 24–33.
[32] P.G. Youssef, S.M. Mahmoud, R.K. Al-Dadah, Performance analysis of four bed adsorption water desalination/refrigeration system, comparison of AQSOA-Z02 to silica-gel, Desalination 375 (2015) 100–107.
[33] H. Wei Benjamin Teo, A. Chakraborty, W. Fan, Improved adsorption characteristics data for AQSOA types zeolites and water systems under static and dynamic conditions, Microporous Mesoporous Mater. 242 (2017) 109–117.
[34] M. Sultan, I.I. El-Sharkawy, T. Miyazaki, et al., Water vapor sorption kinetics of polymer based sorbents: theory and experiments, Appl. Therm. Eng. 106 (2016) 192–202.
[35] M. Sultan, I.I. El-Sharkawy, T. Miyazaki, et al., Insights of water vapor sorption onto polymer based sorbents, Adsorption 21 (3) (2015) 205–215.
[36] K.C. Ng, M. Burhan, M.W. Shahzad, et al., A universal isotherm model to capture adsorption uptake and energy distribution of porous heterogeneous surface, Sci Rep 7 (1) (2017) 10634.
[37] A.S. Uyun, T. Miyazaki, Y. Ueda, et al., High performance cascading adsorption refrigeration cycle with internal heat recovery driven by a low grade heat source temperature, Energies 2 (4) (2009) 1170–1191.
[38] A.S. Alsaman, A.A. Askalany, K. Harby, et al., Performance evaluation of a solar-driven adsorption desalination-cooling system, Energy 128 (2017) 196–207.
[39] M. Thommes, K. Kaneko, A.V. Neimark, et al., Physisorption of gases, with special reference to the evaluation of surface area and pore size distribution (IUPAC Technical Report), Pure Appl. Chem. 87 (9–10) (2015) 1051–1069.
[40] E. Elsayed, R. Al-Dadah, S. Mahmoud, et al., CPO-27(Ni), aluminium fumarate and MIL-101(Cr) MOF materials for adsorption water desalination, Desalination 406 (2017) 25–36.
[41] The evaluation of direct cooling and heating desiccant device coated with FAM.
[42] X. Xia, Z. Liu, S. Li, Adsorption characteristics and cooling/heating performance of COF-5, Appl. Therm. Eng. 176 (2020), 115442.
[43] X. Liu, X. Wang, F. Kapteijn, Water and metal–organic frameworks: from interaction toward utilization, Chem. Rev. 120 (16) (2020) 8303–8377.
[44] Y. Bai, Y. Dou, L.H. Xie, et al., Zr-based metal-organic frameworks: design, synthesis, structure, and applications, Chem Soc Rev 45 (8) (2016) 2327–2367.
[45] V. Bon, I. Senkovska, J.D. Evans, et al., Insights into the water adsorption mechanism in the chemically stable zirconium-based MOF DUT-67 – a prospective material for adsorption-driven heat transformations, J. Mater. Chem. A 7 (20) (2019) 12681–12690.
[46] X. Xia, M. Cao, Z. Liu, et al., Elucidation of adsorption cooling characteristics of Zr-MOFs: effects of structure property and working fluids, Chem. Eng. Sci. 204 (2019) 48–58.